



ELSEVIER

Available online at www.sciencedirect.com

SCIENCE @ DIRECT®

Earth and Planetary Science Letters 213 (2003) 149–167

EPSL

www.elsevier.com/locate/epsl

Re-examination of crystal ages in recent Mount St. Helens lavas: implications for magma reservoir processes[☆]

Kari M. Cooper^{*}, Mary R. Reid¹

Department of Earth and Space Sciences, UCLA, 595 Charles Young Drive East, Los Angeles, CA 90095, USA

Received 15 November 2002; received in revised form 14 February 2003; accepted 30 April 2003

Abstract

U-series data for recent Mount St. Helens lavas suggest that crystallization preceded eruption by more than 0.5 ka but are complicated by possible evidence of crystal recycling and/or addition of radium to the liquid after crystallization. We report new ion and electron microprobe trace- and major-element data for plagioclase and pyroxene in these recent Mount St. Helens lavas and use these data to reassess ^{226}Ra – ^{230}Th crystal ages by taking into account differences in the partitioning behavior of radium and barium and the effects of impurities in mineral separates. Revised ^{226}Ra – ^{230}Th model crystallization ages are ~ 2 – 4 ka for plagioclase (with the exception of the 1982 dacite) and ~ 0.15 – 5.7 ka for pyroxene. In contrast to previous interpretations, no late-stage addition of Ra to the liquid after precipitation of the minerals is required. The variability of Ba concentrations measured in plagioclase is too large to be consistent with progressive crystallization from the same liquid or with diffusive re-equilibration of xenocrysts with a new host liquid. Ba heterogeneity limits the residence time of the crystals in a magma at high temperatures and also suggests that in most cases Ra–Th ages have not been significantly modified by Ra diffusion into or out of the crystals. High (^{226}Ra)/Ba in plagioclase in the 1982 dacite relative to the host liquid likely reflects crystallization processes that precluded bulk crystal–liquid chemical equilibrium. One possibility is that of growth entrapment of surface enrichments during rapid crystallization, which could lead to less discrimination between Ra and Ba than predicted by calculated bulk partition coefficients. ^{226}Ra – ^{230}Th crystal ages for the Castle Creek andesite and basalt that are younger than ^{230}Th – ^{238}U ages of the same crystals could be explained by mixing of crystals into melts with different $^{230}\text{Th}/^{232}\text{Th}$ ratios, by combinations of older and younger crystal growth within the same magma, or, for the basalt, by diffusion of Ra into crystals at high magmatic temperatures. Average plagioclase ages in most of the samples of >2 ka imply that some significant mass fraction of the crystals in each flow was present simultaneously beneath the volcano. This observation could be consistent either with simultaneous storage of physically distinct magma batches or with incorporation of a population of similarly aged crystals into each successive magma batch.

© 2003 Elsevier Science B.V. All rights reserved.

^{*} Corresponding author. Present address: Division of Geological and Planetary Sciences, California Institute of Technology, MC170-25, 1200 East California Boulevard, Pasadena, CA 91125, USA. Tel.: +1-626-395-6145; Fax: +1-626-568-0935.

E-mail address: cooper@gps.caltech.edu (K.M. Cooper).

[☆] Supplementary data associated with this article can be found at doi:10.1016/S0012-821X(03)00262-0

¹ Present address: Department of Geology, Northern Arizona University, Flagstaff, AZ 86011, USA.

Keywords: uranium-series disequilibria; radium; barium; plagioclase; crystallization; diffusion

1. Introduction

Magmatic time scales are fundamentally important in understanding the dynamics of magma systems. Disequilibria between ^{226}Ra ($t_{1/2} = 1600$ yr) and its immediate parent, ^{230}Th , provide a unique opportunity to quantify rates of magmatic processes that have occurred on time scales of ~ 100 to ~ 8000 yr before present, which appears on the basis of studies of whole-rock samples to be commensurate with the duration of magma transport and storage in many mafic to intermediate systems (e.g. [1–6]). However, more precise inferences about magma transport and residence times using this method are limited by the fact that the magnitude of initial ^{226}Ra – ^{230}Th disequilibrium generated during melting is not generally known. Another approach is to use ^{226}Ra – ^{230}Th disequilibria for internal (mineral–mineral and mineral–melt) isochron studies, where the age of phenocryst formation is inferred to provide a measure of the minimum magmatic storage time (e.g. [7–10]). Widespread use of this technique has been limited, partly because the analyses are difficult and partly because the results do not always fit the expected patterns on ^{226}Ra – ^{230}Th –Ba isochron diagrams, wherein Ba is used as a tracer of Ra initially present in the minerals.

In their study of Holocene lavas from Mount St. Helens, Volpe and Hammond [9] (hereafter referred to as V&H91) obtained crystallization ages of 0.5–5 ka before eruption based on ^{226}Ra – ^{230}Th mineral–mineral isochrons (Fig. 1). However, the groundmass of each sample had higher concentrations of ^{226}Ra than would be predicted by reference to $^{226}\text{Ra}/\text{Ba}$ in the minerals. Furthermore, in two of their samples (MSH 90-5 and MSH 90-2), large discrepancies between ages calculated from ^{226}Ra – ^{230}Th and from ^{230}Th – ^{238}U disequilibria appeared to require open-system behavior. V&H91 proposed that late-stage addition of ^{226}Ra to the melt had occurred by assimilation of volatiles and/or fluids; entrainment of older crystals in more ^{226}Ra -enriched ('younger') melt

could also explain these relationships (e.g. [9,11]). Our work on minerals from a recent eruption of Kilauea volcano in Hawaii [10] has demonstrated that, as predicted by an elastic-strain partitioning model [12,13], initial $^{226}\text{Ra}/\text{Ba}$ in the minerals was likely not the same as that in the melt from which they crystallize. Besides potentially leading to erroneous conclusions about crystal ages, variations in initial ($^{226}\text{Ra}/\text{Ba}$) also make ages inferred from isochrons sensitive to the presence of impurities in the mineral separates. To more effectively evaluate the Mount St. Helens mineral data, we obtained new major and trace element compositional data for minerals in thin sections of the same samples analyzed previously (V&H91) and accounted for both the effects of impurities in the mineral separates and differential partitioning of Ra and Ba. With one exception, the ^{226}Ra – ^{230}Th disequilibria between minerals and whole rock/groundmass can now be satisfactorily explained by crystal growth. The differences between ^{226}Ra – ^{230}Th and ^{230}Th – ^{238}U ages remain and we show that they may be explained with mixtures of crystals or zones of different ages within the mineral separates.

2. Samples and methods

The eruptive history of Mount St. Helens has been described in detail elsewhere (e.g. [14–16]). Briefly, the history of the volcano has been divided into five eruptive stages, separated by dormant intervals of thousands of years, which are (from oldest to youngest) the Ape Canyon (~ 35 to < 50 ka), Cougar (~ 18 – 21 ka), Swift Creek (> 9 – 13 ka), Spirit Lake (~ 0.1 – 4 ka), and Current (1980–1986 AD) stages [15]. Within the Spirit Lake and Current stages, the stratigraphy has been further divided into eruptive periods separated by dormant intervals of hundreds of years. The present study concerns lavas erupted within the past ~ 2.5 ka, during (from oldest to youngest) the Castle Creek, Sugar Bowl, and Kalama

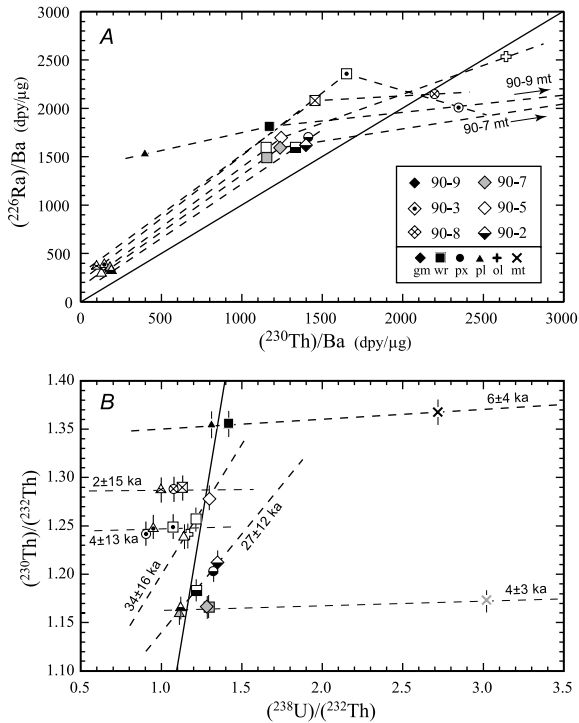


Fig. 1. ^{226}Ra – ^{230}Th (A) and ^{230}Th – ^{238}U isochron (B) diagrams for recent Mount St. Helens samples, constructed using data from Volpe and Hammond [9] (data shown are not corrected for impurities in the mineral separates). Symbols for different samples and phases are shown in the legend. Dashed lines connect points for individual samples and lines in panel B are labeled with apparent ^{230}Th – ^{238}U ages. ^{226}Ra – ^{230}Th ages calculated using different assumptions are given in Table 3. Note that kinked lines in panel A are inconsistent with closed-system crystallization and decay if minerals at the time of crystal growth had $(^{226}\text{Ra})/\text{Ba}$ equal to that in the liquid. See text for discussion.

periods of the Spirit Lake stage, and the Current stage. The samples used in this study were provided by A.M. Volpe and are those described in V&H91. The samples were all erupted effusively and include a range of compositions from olivine basalt to dacite. Eruptive periods, eruption ages, bulk compositions, and previous U-series results (V&H91) are summarized in the Appendix.

To better interpret the U-series results (V&H91) for the mineral separates, we performed electron microprobe and ion microprobe analyses of plagioclase and pyroxene grains in polished thin sections from the same samples. Grains for analysis were selected with reference to backscat-

tered-electron images of the thin sections, and locations of ion microprobe analyses were chosen to be roughly representative of the textural variations and major-element compositions of grains in the thin section. Because the size fraction of the mineral separates analyzed in the previous study by V&H91 was 106–180 μm , we did not analyze any grains whose longest dimension was smaller than $\sim 100 \mu\text{m}$.

Methods used for determining Th and Ba concentrations by ion microprobe analyses were slightly modified from those described in Cooper et al. [10], and for four of the six samples we also obtained U concentrations using the same methods. As before, counts of ^{232}Th and ^{138}Ba were normalized to ^{28}Si , and concentrations were calculated relative to the mean of several analyses of a glass standard (WU-A) obtained during the same analysis session as the unknowns. For unknowns, Si concentrations were taken from individual electron microprobe analyses of the same spot or zone within the crystal. Samples were run with 20–50 nA primary beam currents ($^{16}\text{O}^-$ beam) at a mass-resolving power of ~ 4000 with a -30 V offset during Ba analysis to minimize molecular interferences, which appear to result from surface contamination. Polished thin sections were coated with gold (MSH 90-9) or carbon (other samples); no systematic differences were found between Au and C coats in either the results for standards analyzed as unknowns or in the abundance of molecular interferences present near Ba peaks. In the present study, $^{30}\text{Si}/^{28}\text{Si}$ and $^{137}\text{Ba}/^{138}\text{Ba}$ ratios were monitored for every unknown analysis, and an energy adjustment before every block was used to consistently maintain the voltage offset on Ba despite sample charging in order to increase precision. Uncertainties in calculated concentrations based on propagation of internal precision of the analyses were generally 5–10% (1σ) for Th measurements, 1–3% for Ba measurements in plagioclase and 5–10% for Ba measurements in pyroxene. Accuracy and reproducibility of Th analyses were estimated by analyses of additional glass standards as unknowns, and were generally within 25% and 15% (2σ), respectively, over five analysis sessions; accuracy and reproducibility of U analyses over

Table 1
Summary of electron microprobe analyses of plagioclase in Mount St. Helens samples

Sample <i>n</i>	MSH 90-9		MSH 90-3		MSH 90-8		MSH 90-7		MSH 90-5		MSH 90-2	
	mean	1 σ										
SiO ₂	56.31	3.16	55.34	2.50	55.22	2.24	57.36	1.71	53.14	2.84	52.70	2.52
Na ₂ O	5.75	1.09	5.12	1.01	5.41	0.93	6.46	0.60	4.52	1.08	4.45	1.07
Al ₂ O ₃	27.2	2.1	27.6	1.6	27.6	1.5	26.8	1.0	29.1	1.9	29.6	1.6
FeO	0.33	0.08	0.64	0.13	0.69	0.08	0.29	0.07	0.63	0.11	0.49	0.11
K ₂ O	0.27	0.21	0.30	0.13	0.25	0.11	0.21	0.07	0.22	0.22	0.14	0.07
CaO	10.0	2.3	10.9	1.9	10.6	1.8	8.8	1.1	12.2	2.2	12.5	1.9
Total	99.84		99.91		99.66		99.89		99.75		99.84	
An	0.482	0.107	0.534	0.092	51.256	8.576	0.425	0.055	0.590	0.106	0.603	0.095
Ab	0.503	0.097	0.449	0.086	47.304	8.002	0.563	0.051	0.397	0.094	0.389	0.092
Or	0.016	0.013	0.017	0.007	1.440	0.612	0.012	0.004	0.013	0.012	0.008	0.004

Error reported as 1 standard deviation of the mean.

three analysis sessions were within $\sim 50\%$ and 10% , respectively, for the glass standard with the lowest concentration (0.07 ppm); therefore, the U analyses reported here should be treated with caution. Reproducibility of $^{138}\text{Ba}/^{28}\text{Si}$ measurements on the standard used for calibration was better than 20% ; although Ba concentrations were not available for the standards analyzed as unknowns, assuming that concentration and therefore count rate is the main control on accuracy, the accuracy of the Ba analyses is likely to be similar to that of the Th analyses in pyroxene and better for plagioclase analyses.

3. Results

Major-element data for plagioclase are summarized in Table 1; averages for a given sample are presented because those are used in the model age calculations. Full data for both plagioclase and pyroxene are presented in Table S1–S9². Data for TIMS analyses of the bulk separates [9] are reproduced in the Appendix². Concentrations of Ba, Th, and U measured in situ by ion microprobe (Table 2) are much lower than those in the bulk mineral separates, as observed in our

results for a Hawaiian lava [10]. This likely indicates impurities in the mineral separates in the form of glass/groundmass in the plagioclase separates and either glass or plagioclase in the pyroxene separates. Concentrations of Ba measured in plagioclase vary by a factor of 4, and correlate inversely with An content (Fig. 2). These variations in Ba concentrations are evident both between samples and within the plagioclase data for a single sample (Fig. 2). The two dacite samples (MSH 90-9 and MSH 90-7) exhibit the widest range in both An and Ba, and the most restricted compositions were measured in the Castle Creek basalt (MSH 90-5), whereas the andesites show intermediate ranges of compositions. In general we avoided analyzing trace elements in multiple spots on the same grain in order to obtain a data set representative of the crystal population as a whole; however, in the few cases where we did, individual plagioclase grains were also found to be heterogeneous in their Ba concentrations (Table 2 and Fig. 2). No systematic variations of Th or U concentration in plagioclase with An or Ba were apparent within the error of the measurements; however, there is a weak correlation of Th with U concentrations (not shown). Similarly, no systematic variation of Ba, Th, or U concentration with pyroxene major-element composition or correlation of Th or U concentrations with Ba concentrations is apparent, but Th and U concentrations are weakly correlated.

² For these tables and the appendix see the online version of this paper.

Table 2
Ion microprobe analyses of plagioclase and pyroxene in Mount St. Helens samples

Sample	An or Mg #	Th		Ba		U	
		ppm	1 S.E.	ppm	1 S.E.	ppm	1 S.E.
<i>MSH 90-9 plagioclase</i>							
MSH90-9_PL1sp1	56.8	0.007	0.0002	84.8	1.3	n.d.	n.d.
MSH90-9_PL5sp1	45.8	0.009	0.0002	87.8	1.4	n.d.	n.d.
MSH90-9_PL3sp1	60.7	0.010	0.0003	34.5	0.5	n.d.	n.d.
MSH90-9_PL7sp1	36.2	0.009	0.0003	84.4	1.2	n.d.	n.d.
MSH90-9_PL25sp1	16.6	0.012	0.0003	213.4	3.0	n.d.	n.d.
MSH90-9_PL26sp1	80.6	0.017	0.0004	53.1	0.8	n.d.	n.d.
MSH90-9_PL26sp2	42.0	0.009	0.0004	165.2	2.4	n.d.	n.d.
MSH90-9_PL30sp1	66.9	0.009	0.0003	42.7	0.7	n.d.	n.d.
MSH90-9_PL30sp2	43.4	0.011	0.0003	153.5	2.4	n.d.	n.d.
MSH90-9_PL31sp1	50.7	0.015	0.0004	92.5	1.4	n.d.	n.d.
MSH90-9_PL36sp1	n.d.	0.015	0.0004	112.6	1.6	n.d.	n.d.
MSH90-9_PL36sp2	n.d.	0.006	0.0002	81.0	1.1	n.d.	n.d.
MSH90-9_PL16sp1	61.8	0.009	0.0003	32.1	0.5	n.d.	n.d.
MSH90-9_PL18sp1	49.6	0.011	0.0003	121.3	1.9	n.d.	n.d.
MSH90-9_PL34sp1	53.9	0.009	0.0003	92.3	1.4	n.d.	n.d.
MSH90-9_PL34sp2	47.2	0.011	0.0004	96.6	1.4	n.d.	n.d.
MSH90-9_PL13sp1	62.0	0.012	0.0005	46.6	0.7	n.d.	n.d.
mean		0.011		93.8			
1 σ mean		0.003		48.9			
<i>MSH 90-3 plagioclase</i>							
MSH3_PL1sp1	56.7	0.005	0.0002	135.6	3.2	n.d.	n.d.
MSH3_PL2sp1	48.0	0.022	0.0006	153.3	3.7	n.d.	n.d.
MSH3_PL3sp1	64.1	0.004	0.0002	58.3	1.1	n.d.	n.d.
MSH3_PL4sp1	47.0	0.008	0.0003	177.8	4.4	n.d.	n.d.
MSH3_PL5sp1	45.1	0.004	0.0002	97.1	2.4	n.d.	n.d.
MSH3_PL5sp2	57.3	0.005	0.0002	110.1	2.6	n.d.	n.d.
MSH3_PL5sp3	52.5	0.004	0.0002	81.1	2.0	n.d.	n.d.
MSH3_PL7sp1	44.5	0.010	0.0003	159.8	3.8	n.d.	n.d.
mean		0.008		121.637			
1 σ mean		0.006		41.7			
<i>MSH 90-3 clinopyroxene</i>							
MSH3_cpx1sp1	75.3	0.020	0.0005	0.050	0.004	n.d.	n.d.
MSH3_cpx1sp2	70.2	0.018	0.0008	0.057	0.004	n.d.	n.d.
MSH3_cpx4sp1	82.3	0.036	0.0009	0.839	0.042	n.d.	n.d.
MSH3_cpx5sp1	82.0	0.017	0.0005	0.210	0.013	n.d.	n.d.
MSH3_cpx6sp1	73.5	0.039	0.0034	0.875	0.059	n.d.	n.d.
MSH3_cpx7sp1	80.2	0.019	0.0004	0.062	0.004	n.d.	n.d.
MSH3_cpx8sp1	n.d.	0.019	0.0004	0.066	0.005	n.d.	n.d.
MSH3_cpx9sp1	80.0	0.019	0.0004	0.049	0.003	n.d.	n.d.
MSH3_cpx10sp1	75.3	0.021	0.0005	0.127	0.004	n.d.	n.d.
MSH3_cpx11sp1	80.7	0.013	0.0004	0.137	0.008	n.d.	n.d.
mean		0.022		0.247			
1 σ mean		0.008		0.3			
<i>MSH 90-3 orthopyroxene</i>							
MSH3_OPX1sp1	n.d.	0.004	0.0002	0.355	0.008	n.d.	n.d.
MSH3_OPX3sp1	70.2	0.008	0.0002	0.356	0.010	n.d.	n.d.
MSH3_OPX6sp1	70.8	0.019	0.0004	0.170	0.008	n.d.	n.d.
mean		0.010		0.293			
1 σ mean		0.008		0.107			
<i>MSH 90-8 plagioclase</i>							
MSH90-8_PL5sp1	51.1	0.013	0.0005	119.4	2.4	0.013	0.0005

Table 2 (Continued).

Sample	An or Mg #	Th		Ba		U	
		ppm	1 S.E.	ppm	1 S.E.	ppm	1 S.E.
MSH90-8_PL8sp1	67.3	0.001	0.0001	44.7	0.9	0.008	0.0005
MSH90-8_PL8sp2	50.7	0.003	0.0002	97.6	1.6	0.010	0.0006
MSH90-8_PL11sp1	57.1	0.002	0.0002	106.7	1.8	0.006	0.0003
MSH90-8_PL11sp2	69.6	0.001	0.0001	41.8	0.7	0.006	0.0004
MSH90-8_PL13sp1	52.1	0.001	0.0001	101.9	2.6	0.005	0.0002
mean		0.003		85.3		0.008	
1 σ mean		0.005		33.4		0.003	
<i>MSH 90-8 pyroxene</i>							
MSH90-8_PX4_sp2	72.9	0.010	0.0004	0.132	0.012	0.011	0.0005
MSH90-8_PX25_sp1	72.3	0.002	0.0002	0.304	0.053	0.005	0.0002
MSH90-8_PX29_sp1	73.6	0.001	0.0002	0.088	0.007	0.008	0.0005
MSH90-8_PX32_sp1	72.8	0.002	0.0002	0.138	0.014	0.009	0.0008
MSH90-8_PX35_sp1	72.4	0.005	0.0003	0.060	0.003	0.009	0.0006
MSH90-8_PX38_sp1	71.2	0.002	0.0002	0.057	0.004	0.006	0.0004
MSH90-8_PX42_sp1	73.9	0.012	0.0005	0.758	0.029	0.011	0.0006
MSH90-8_PX44_sp1	72.9	0.019	0.0008	0.138	0.011	0.014	0.0009
mean		0.007		0.209		0.009	
1 σ mean		0.007		0.235		0.003	
<i>MSH 90-7 plagioclase</i>							
MSH90-7_PL1sp1	46.4	0.003	0.0002	113.9	2.2	0.004	0.0006
MSH90-7_PL5sp1	58.8	0.005	0.0002	54.2	1.1	0.011	0.0007
MSH90-7_PL17sp1	53.2	0.002	0.0002	44.0	0.9	0.002	0.0004
MSH90-7_PL17sp2	53.0	0.002	0.0001	127.3	2.5	0.002	0.0004
MSH90-7_PL19sp1	36.6	0.002	0.0001	159.4	3.2	0.003	0.0004
MSH90-7_PL22sp1	37.2	0.019	0.0007	154.1	3.0	0.034	0.0019
MSH90-7_PL24sp1	43.7	0.002	0.0001	159.4	3.6	0.002	0.0004
MSH90-7_PL25sp1	38.9	0.002	0.0002	151.1	3.0	0.003	0.0005
MSH90-7_PL26sp1	40.1	0.005	0.0002	145.8	2.9	0.011	0.0007
MSH90-7_PL33sp1	29.5	0.003	0.0002	167.5	3.2	0.010	0.0006
mean		0.005		127.7		0.008	
1 σ mean		0.005		44.4		0.010	
<i>MSH 90-5 plagioclase</i>							
MSH90-5_PL1sp1	66.9	0.014	0.0003	59.1	0.6	0.007	0.0004
MSH90-5_PL6sp1	62.6	0.003	0.0001	65.3	0.6	0.003	0.0002
MSH90-5_PL7sp1	64.6	0.003	0.0001	57.0	0.6	0.003	0.0002
MSH90-5_PL11sp1	61.6	0.006	0.0001	53.2	0.5	0.005	0.0002
MSH90-5_PL12sp1	62.3	0.003	0.0001	54.9	0.6	0.004	0.0002
MSH90-5_PL16sp1	57.8	0.003	0.0001	89.9	0.8	0.003	0.0002
MSH90-5_PL19sp1	63.0	0.005	0.0001	64.2	0.7	0.004	0.0002
MSH90-5_PL21sp1	65.2	0.003	0.0001	50.7	0.5	0.003	0.0002
MSH90-5_PL23sp1	65.9	0.002	0.0001	56.4	0.5	0.003	0.0002
MSH90-5_PL24sp1	62.8	0.006	0.0001	59.3	0.6	0.004	0.0002
mean		0.005		61.0		0.004	
1 σ mean		0.003		11.1		0.001	
<i>MSH 90-2 plagioclase</i>							
MSH90-2_pl3sp1	51.0	0.002	0.0001	113.2	3.6	0.001	0.0003
MSH90-2_pl3sp2	61.0	0.002	0.0001	44.2	1.5	0.001	0.0003
MSH90-2_pl4sp1	63.9	0.002	0.0002	44.5	1.5	0.001	0.0003
MSH90-2_pl11sp1	64.3	0.002	0.0001	38.3	1.4	0.001	0.0002
MSH90-2_pl13sp1	69.6	0.002	0.0001	44.8	1.3	0.001	0.0002
MSH90-2_pl14sp1	60.4	0.002	0.0001	75.3	3.3	0.001	0.0003
MSH90-2_pl22sp1	78.2	0.002	0.0001	39.8	1.1	0.001	0.0003
MSH90-2_pl24sp2	72.6	0.003	0.0002	53.2	1.8	0.002	0.0002

Table 2 (Continued).

Sample	An or Mg #	Th		Ba		U	
		ppm	1 S.E.	ppm	1 S.E.	ppm	1 S.E.
mean		0.002		56.7		0.001	
1 σ mean		0.0003		25.7		0.0003	
<i>MSH 90-2 clinopyroxene</i>							
MSH90-2_px3sp1	71.6	0.035	0.0008	0.114	0.0069	0.014	0.0009
MSH90-2_px6sp1	73.3	0.020	0.0005	0.399	0.0096	0.008	0.0010
MSH90-2_px10sp1	73.9	0.018	0.0005	0.145	0.0051	0.008	0.0008
mean		0.024		0.219		0.010	
1 σ mean		0.0096		0.156		0.0031	
<i>MSH 90-2 orthopyroxene</i>							
MSH90-2_px1sp1	64.3	0.005	0.0002	0.130	0.0037	0.003	0.0003
MSH90-2_px2sp1	73.2	0.002	0.0001	0.038	0.0100	0.001	0.0002
MSH90-2_px9sp1	67.9	0.010	0.0003	0.037	0.0039	0.003	0.0003
MSH90-2_PX10sp2	71.9	0.001	0.0001	0.045	0.0066	0.001	0.0002
MSH90-2_px13sp1	71.5	0.006	0.0003	0.194	0.0237	0.003	0.0005
mean		0.005		0.089		0.002	
1 σ mean		0.0037		0.071		0.0010	

4. Discussion

4.1. Ba in plagioclase: implications for crystal histories

The inverse relationship between Ba and An content of the Mount St. Helens feldspar (Fig. 2) is qualitatively that expected based on the systematic variation in partitioning behavior of Ba between plagioclase and silicate melt with the major-element composition of the plagioclase [12]. The feldspar data cluster around equilibrium concentrations predicted for plagioclase crystallizing from liquids with Ba contents like those of the lavas (250–350 ppm) at temperatures of 1100–900°C. However, there is more variability of Ba at any given An content than could be explained by progressive crystallization of plagioclase from the same liquid, especially considering that the effects on plagioclase of increasing Ba in the liquid with increasing differentiation will be offset by the predicted decrease in D_{Ba} with decreasing temperature (Fig. 2). Furthermore, each of the dacites and andesites contains some calcic plagioclase with relatively low Ba (which would be in equilibrium with a liquid with ~ 150 ppm Ba). These observations support the consensus from previous work that plagioclase crystals in Mount St. Helens lavas have complex histories and may include

a component recycled from earlier episodes of magmatism (e.g. [11,17]). One exception to this general observation is that plagioclase compositions are more restricted in the Castle Creek basalt sample (MSH 90-5) than in other samples and are broadly consistent with crystallization of plagioclase from a magma with 250 ppm Ba at $\sim 1000^\circ\text{C}$.

The variability in plagioclase Ba concentrations in the majority of the MSH samples is also evidence that the temperatures and/or time scales of plagioclase residence in their host liquids prior to eruption were not high enough and/or long enough, respectively, to allow diffusive equilibration of Ba with the host. This is especially evident in the pairs of points from single plagioclase grains, where in almost all cases tie-lines between the points cross the model Ba–An curves in Fig. 2 transverse to the temperature contours, and transverse to the direction of increasing fractionation (in the simple scenario where fractionation leads to decreasing An). This indicates that Ba in different zones within a single crystal has not diffusively equilibrated within the crystal or with the same – even if evolving – host liquid. Diffusivity of Ba in plagioclase has recently been measured experimentally [18], and we use these measurements to assess the time scale of diffusive equilibration of Ba at magmatic temperatures relevant to the

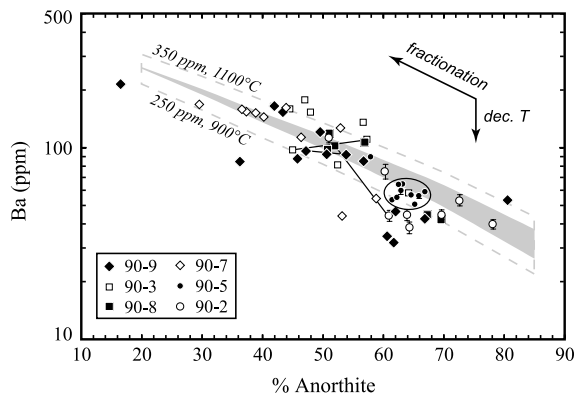


Fig. 2. Barium concentration measured in plagioclase in recent Mount St. Helens lavas by ion microprobe (Table 2) plotted against major-element composition of plagioclase (%An); error bars shown where larger than the symbols. Analyses of plagioclase in different samples are distinguished by different symbols (MSH 90-X; see legend). Data points for all but one analysis of the Castle Creek basalt (MSH 90-5) are enclosed within a field. The elongated gray field represents the concentration of Ba in plagioclase at a given %An predicted to be in equilibrium with a liquid with 300 ppm Ba at 1100–900°C (upper and lower bounds of this field, respectively) based on calculated partition coefficients [20]. Dashed gray lines enclose the field of expected compositions of plagioclase crystallizing from liquids with 250–350 ppm Ba over the same temperature range. Note that while these fields are not calculated fractionation paths, arrows in upper right corner show general trends expected in the case where progressive fractionation leads to higher Ba in the liquid and lower An in plagioclase crystallizing from that liquid ('fractionation') and in the case of decreasing temperature without changing composition ('dec. T'). Errors in accuracy of calculated partition coefficients are likely to be systematic and will shift the fields up or down without greatly changing the slope. Also shown (fine black tie-lines) are examples of pairs of points measured in the same crystal where the variation in Ba with An is inconsistent with equilibrium with the same (or even an evolving) liquid. See text for discussion.

Mount St. Helens samples (900–1200°C). The Castle Creek basalt (MSH 90-5) could have had pre-eruptive temperatures greater than 1100°C, and plagioclase in this sample is more homogeneous in Ba concentration than that in the other samples. At these temperatures, Ba concentrations in volumes close to the rim (within 50–100 μm , as is the case for many of the ion microprobe spots) would have equilibrated with their host liquid within hundreds to thousands of years, even if multiple plagioclase populations are present in this lava (M. Clynné, personal communication),

each with Ba concentrations originally in equilibrium with a different liquid. Conversely, we do observe significant scatter in the Ba–An covariations exhibited by the other samples over ~ 50 – $100 \mu\text{m}$ length scales, which suggests, in turn, that the plagioclase could not have resided in magmas at temperatures in excess of 1000°C for more than ~ 7 kyr but could have resided for longer time periods (tens to hundreds of thousands of years) at lower temperatures. Beyond providing some constraints on the duration of crystal storage in a magma, the lack of Ba–An equilibrium helps to assess the extent to which ^{226}Ra – ^{230}Th ages may have been affected by diffusion (cf. [18]). In addition to the chemical potential produced by introducing crystals that grew from one liquid into a liquid with a different Ra concentration, a chemical potential between crystals and liquid might be created simply by decay of Ra in crystals during magma storage. Low Ra in crystals relative to that in equilibrium with the melt, whether produced by decay or by entrainment of crystals in a melt with relatively high Ra, would result in diffusion of Ra into the crystals, whereas entrainment by a magma with low Ra would result in diffusion out of the crystals. As a result, ^{226}Ra – ^{230}Th apparent ages may be either younger or older than crystallization ages as a result of diffusion. At 1000°C, Ba and Ra diffusion rates in both diopside and plagioclase are estimated to be similar, based on calculations using the model of Van Orman et al. [19] and the experimental work of Cherniak [18]. Thus, the preservation of Ba zoning in plagioclase that is not in equilibrium with the host liquid is evidence that ages obtained from ^{230}Th – ^{226}Ra disequilibrium in the Mount St. Helens samples may not have been appreciably affected by Ra diffusion, with the possible exception of the Castle Creek basalt (MSH 90-5).

4.2. Re-examination of Ra–Th ages

In this section, we present new Ra–Th model ages for the Mount St. Helens samples and compare these new ages to mineral–mineral ages reported previously for the same lavas (V&H91). The ages reported here incorporate the significant difference in the ability of Ra and Ba to substitute

for Ca in plagioclase and pyroxene [12,13], whereas those of V&H91 were based on the assumption that Ba is a perfect chemical analog for Ra during mineral growth (Table 3). In order to correct for differences due to partitioning effects, we use the approach that we have described previously [10].

We correct for the effects of impurities in the mineral separates by mass-balance calculations in which the Th and Ba concentrations of the pure mineral phases (obtained by ion microprobe analyses) are used to constrain the Ra concentrations in the pure minerals (see legend to Table 3

Table 3
Summary of U-series ages

Samples used in age calculations	V&H91 isochron ages ^a		Ra–Th model ages (this study)		
	U–Th ages	Ra–Th ages	Corrected for impurities only ^b	Corrected for impurities and Ra–Ba fractionation ^c	Fixed initial (²²⁶ Ra)/Ba in liquid ^d
<i>MSH 90-9 (1982 AD)</i> isochron/consensus ^e plagioclase–whole rock	6 ± 4	0.5 (pl–mt)	1.7	< 1.7 ^f	n/a
<i>MSH 90-3 (0.43–0.48 ka)</i> isochron/consensus plagioclase–whole rock pyroxene–whole rock	4 ± 13	3.0 (pl–px) undefined	undefined (pl–px) ^g undefined undefined	no overlap 4.8 to > 8 (6.0) 0.15–3.2	1.5
<i>MSH 90-8 (0.43–0.48 ka)</i> isochron/consensus plagioclase–whole rock pyroxene–whole rock	2 ± 15	4.5 (pl–px) undefined	undefined (pl–px) undefined	2.4–4.4 2.4–4.4 (3.0)	1.1
<i>MSH 90-7 (1.1 ka)</i> isochron/consensus plagioclase–groundmass	4 ± 3	1.0 (pl–mt) undefined	1.0 (pl–mt) undefined	n/a 3.3–5.2 (3.8)	2.3
<i>MSH 90-5 (~1.7 ka)</i> isochron/consensus plagioclase–groundmass	34 ± 16	5.0 (pl–ol) undefined	5.2 (pl–ol) undefined	n/a 2.1–3.7 (2.9)	1.4
<i>MSH 90-2 (1.7–2.1 ka)</i> isochron/consensus plagioclase–groundmass pyroxene–groundmass	27 ± 12	undefined (< 10 ka) undefined	undefined **	n/a 2.8–4.1 (3.2) **	2.4

All ages calculated as kyr before 1990 (date of analysis).

^a Ages as reported by V&H91 except for the mineral–whole rock/groundmass ages which we calculated from their data; ages are not corrected for impurities or for fractionation of Ra from Ba during mineral growth.

^b Ra concentrations for the impurities are estimated from Ra abundance measured by TIMS in the groundmass/whole rock and/or in the plagioclase separates. Pyroxene impurities in the plagioclase bulk separate will have a negligible effect on the calculated concentration of Ra in pure plagioclase and therefore all impurities are inferred to be groundmass/inclusions. Plagioclase impurities in pyroxene separates could account for a significant part of the Ra and Ba budgets of the bulk separate, although the contribution of plagioclase to the Th content of the bulk separate will be negligible. We therefore infer that the difference between TIMS and ion microprobe measurements of Th in pyroxene (and a corresponding part of the difference in Ba concentrations) is due to the presence of glass inclusions/groundmass, and that plagioclase accounts for any remaining ‘excess’ Ba in the TIMS measurement.

^c Uncertainties in pyroxene model ages from this study primarily reflect uncertainties in mass-balance calculations rather than uncertainties in calculated partition coefficients. Pyroxene model ages for MSH 90-2 (double asterisk) are not reported because overlap between pyroxene and groundmass data does not allow correction for impurities.

^d Ages of plagioclase calculated by assuming an initial (²²⁶Ra)/Ba in the liquid of 1000 dpm/mg; ages shown here are minimum ages given uncertainties in An content and temperature is similar to age ranges in column immediately to left.

^e Isochron ages are calculated from mineral–mineral slopes (minerals used indicated in parentheses); consensus ages are calculated from overlap in pyroxene and plagioclase model ages.

^f Age calculated allowing for growth entrapment; see text for details.

^g Undefined ages are those where the two-point slope is either greater than one or less than zero.

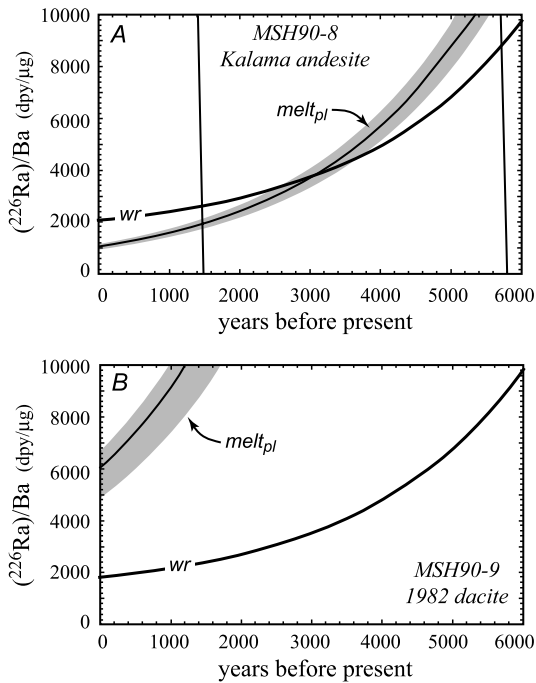


Fig. 3. Example evolution diagrams for Mount St. Helens samples; diagrams for the remaining samples are presented in Figure S1². (A) MSH 90-8 (Kalama andesite), which is similar to evolution diagrams for all samples except MSH 90-9. Curves are shown for $(^{226}\text{Ra})/\text{Ba}$ at times in the past for whole rock (wr) and for melt in equilibrium with plagioclase (melt_{pl}) and pyroxene (near-vertical lines). Two curves for pyroxene reflect maximum and minimum Ra concentrations in pure pyroxene allowed by uncertainties in mass-balance. Curve for melt in equilibrium with plagioclase represents the best estimate based on average of measured plagioclase compositions (An_{50}) and estimated pre-eruptive temperature of 1000°C; gray field encloses composition of melt in equilibrium with plagioclase allowing for variations in An ($\pm \text{An}_{10}$) and temperature (1000–1100°C). Model ages are calculated from intersections of curves for melt in equilibrium with minerals with evolution curve for whole rock. The extremely low concentrations of Th in plagioclase relative to Ra lead to decay of Ra that is relatively rapid compared to that of Ra in the liquid, which is partially supported by decay of ^{230}Th . (B) 1982 dacite (MSH 90-9). As in panel A, melt in equilibrium with plagioclase calculated from average of measured plagioclase compositions (An_{50}) and estimated pre-eruptive temperature of 900°C; gray field encloses composition of melt in equilibrium with plagioclase allowing for variations in An ($\pm \text{An}_{10}$) and temperature (900–1000°C). Note that model age is “undefined” (see Table 3) because curves for evolution of melt in equilibrium with plagioclase and for whole rock do not intersect. See text for discussion.

for details). Calculated partition coefficients are then used to predict $(^{226}\text{Ra})/\text{Ba}$ in a hypothetical liquid in chemical equilibrium with the phases at any given time in the past (Fig. 3). Model crystallization ages for plagioclase and pyroxene are obtained from the point in time where the decay-corrected $(^{226}\text{Ra})/\text{Ba}$ in the liquid in equilibrium with the minerals matches that in the groundmass separate and/or whole rock, represented graphically by the intersection point between the two curves in Fig. 3; these ages are summarized in Table 3 and Fig. 4. We consider these to be model ages because they are based on the assumptions that the composition of the groundmass and/or whole rock is representative of the liquid from which the minerals grew, that changes in ^{226}Ra

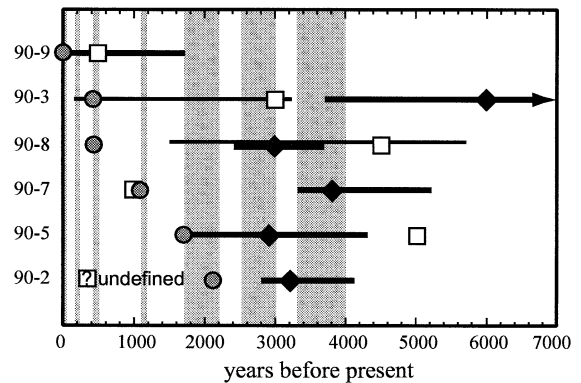


Fig. 4. Summary of ^{226}Ra – ^{230}Th ages for Mount St. Helens samples. Filled diamonds represent ‘best-estimate’ plagioclase model ages considering the effects of inclusions and of differential partitioning of Ra and Ba, using mean plagioclase compositions and temperatures as follows: MSH 90-9, An_{50} , 900°C; MSH 90-3, An_{50} , 1000°C; MSH 90-8, An_{50} , 1000°C; MSH 90-7, An_{40} , 900°C; MSH 90-5, An_{60} , 1100°C; MSH 90-2, An_{60} , 1000°C. Bold lines indicate range of plagioclase model ages allowing for variations in An ($\pm \text{An}_{10}$) and temperature (900–1000°C for dacites, 1000–1100°C for andesites, and 1000–1200 for the basalt). Arrow pointing to right for MSH 90-3 plagioclase age indicates that the upper limit is > 8 ka. Ranges of pyroxene model ages (90-3 and 90-8 only) are shown by fine lines; these ranges primarily reflect propagation of uncertainties through mass-balance calculations of Ra in pure pyroxene; uncertainties in model $D_{\text{Ra}}/D_{\text{Ba}}$ have a very minor effect (cf. [10]). Gray circles represent eruption ages for each sample (sample numbers along vertical axis), open squares represent mineral–mineral isochron ages calculated by V&H91. Shaded vertical bands represent periods of eruptive activity [14,15].

(and ^{230}Th) in the liquid and mineral phases are solely the result of in situ decay, and that partitioning behavior is as predicted from theory.

Age ranges presented in Table 3 and Fig. 4 indicate uncertainties in the average crystal ages due to variation in measured crystal compositions, uncertainties in calculated partition coefficients, and uncertainties in estimated crystallization temperatures, rather than the duration of crystallization. Even considering these uncertainties, our model ages for plagioclase do not in general agree with the mineral–mineral ages calculated by V&H91, but they are neither consistently older nor younger (Fig. 4). In part this could reflect the fact that V&H91 did not correct for the effects of groundmass impurities in the mineral separates; because the groundmass data are not collinear with the mineral data on the isochron diagram this must have skewed the mineral–mineral ages to some degree. Moreover, even had they corrected for impurities but not for Ra–Ba fractionation, pyroxene–plagioclase ages for MSH 90-3 and MSH 90-8 would have been undefined, just as was the case for plagioclase–whole-rock/groundmass ages whether corrected for impurities or not (Table 3). When the effects of differential partitioning of Ra and Ba are also considered, we obtain sensible model ages for plagioclase from all but one sample (the 1982 dacite; MSH 90-9) assuming crystallization from liquids with $(^{226}\text{Ra})/\text{Ba}$ like those recently erupted from Mount St. Helens. A first-order conclusion from our re-evaluation of these data is thus that no late-stage addition of Ra is required to explain the data.

Model ages are presented for pyroxene and plagioclase separately because it is possible or even likely, given the evidence for crystal recycling presented above and in previous work [11,17] (also M. Clyne, personal communication), that the average ages of pyroxene and plagioclase populations in the same sample are different. The model crystal ages are relatively robust even considering possible crystal recycling, because allowing $(^{226}\text{Ra})/\text{Ba}$ in the liquid to vary across the entire range of whole-rock/groundmass values [9] will not greatly affect the calculated ages. Average ages of plagioclase in all but the 1982 dacite over-

lap significantly, and are greater than ~ 2 ka. The age of plagioclase in the 1982 dacite sample (MSH 90-9) is undefined (apparently negative), the significance of which will be discussed below. Average ages of pyroxene in the Kalama andesites (MSH 90-3 and MSH 90-8) are 0.15–3.3 ka and 1.5–5.7 ka, respectively (Table 3 and Fig. 4). A ‘consensus’ age assuming co-precipitation of pyroxene and plagioclase in MSH 90-8 would be 2.4–4.4 ka, while there is no overlap of the average plagioclase and pyroxene ages in MSH 90-3 (Table 3 and Fig. 4).

An implicit assumption in the foregoing model ages is that each liquid aged for essentially the same amount of time as the average age of the crystals it contains, even if not all of the crystals precipitated from that liquid. An alternative scenario would be that magmas are relatively transient features of the plumbing system and that crystallization times are short, and therefore that the crystals that are not of near-eruption age did not precipitate from their host liquid. For this case, $(^{226}\text{Ra})/\text{Ba}$ ratios in the liquids at the time of eruption may be more representative of the transient liquids from which the minerals crystallized. An alternative set of ages is therefore presented in Table 3 for which the minerals are corrected to an initial $(^{226}\text{Ra})/\text{Ba}$ in equilibrium with a liquid with $(^{226}\text{Ra})/\text{Ba}$ of 1800 disintegrations per year (dpy)/ μg , the lowest eruption-age $(^{226}\text{Ra})/\text{Ba}$ obtained for a recent MSH lava. Model ages for pyroxene do not change appreciably using this alternative assumption due to the steep evolution curves. The resulting model plagioclase ages are minimum ages and are somewhat lower than those calculated above, ranging from 1.1 to 2.4 ka (Table 3); with only one exception (MSH 90-5), these ages are still hundreds of years to more than 1 kyr before eruption.

The model mineral age represents an average for the bulk separate which, to a first approximation, is equivalent to a volume-averaged age of crystallization. For the plagioclase ages, considering the variations in Ba concentrations within plagioclase crystals (Fig. 2), there is likely to have been some variability in initial Ra concentration in plagioclase and thus in the contribution of each crystal or zone to the bulk age, but given the

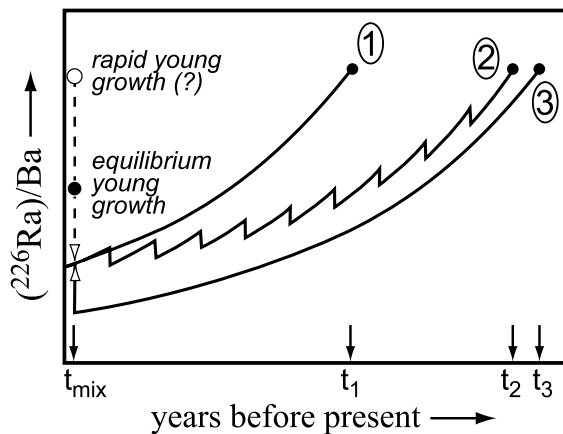


Fig. 5. Schematic diagram showing effects of progressive and/or episodic crystallization on calculated model ages. The measured $(^{226}\text{Ra})/\text{Ba}$ in plagioclase separates could reflect several possibilities each of which yields the same present-day $(^{226}\text{Ra})/\text{Ba}$: (1) The measured $(^{226}\text{Ra})/\text{Ba}$ reflects crystallization at a single point in the past (the model age, t_1) followed by closed-system decay. (2) Crystallization is episodic, beginning at t_2 , and $(^{226}\text{Ra})/\text{Ba}$ in the bulk separate, which represents a mixture of old and young crystals, is maintained at a higher level than would be the case for simple decay. (3) One population of crystals formed early (t_3), and followed a closed-system decay path until mixed with a young crystal component (e.g. by overgrowths on the old cores) shortly before eruption (t_{mix}). In scenarios 2 and 3, $(^{226}\text{Ra})/\text{Ba}$ measured in the mineral separate will be a weighted average of that in the crystal populations (and/or zones within individual crystals) of different ages and the model age (t_1) will be intermediate between the onset of crystallization and the final episode(s) of crystallization. Because of exponential decay of ^{226}Ra in any old crystal material, the model age in these scenarios will not be a simple mean age of crystallization but rather will be weighted towards younger crystal growth.

overall uncertainty in the model ages this will be a minor effect. The model ages could be interpreted either as the time of a ‘burst’ of crystallization, if most of the crystals in the rock formed within a short period of time (a few tens to hundreds of years), or as a weighted average age of more progressive crystal growth, whether episodic or continuous (Fig. 5).

4.3. Potential effects of rapid crystallization

4.3.1. 1982 dacite (MSH 90-9)

On the evolution diagram in Fig. 3, $(^{226}\text{Ra})/\text{Ba}$ predicted for a melt in equilibrium with the 1982

plagioclase is everywhere higher than that in the whole rock: hence, plagioclase model ages calculated using our method for the 1982 dacite dome (MSH 90-9) are undefined (negative). $(^{226}\text{Ra})/\text{Ba}$ in the 1982 plagioclase is also anomalously high compared to the other samples when plotted on a conventional ^{226}Ra – ^{230}Th isochron diagram (Fig. 1A). This effect cannot simply be attributed to a high percentage of glass impurities in the 1982 dacite plagioclase separate because Th/Ba in pure plagioclase measured by ion microprobe is similar to that in other samples, whereas $(^{226}\text{Ra})/\text{Ba}$ is still much higher after correcting for impurities. There are two possible explanations for the pattern of data shown in Fig. 3A: either plagioclase in the 1982 dacite did not precipitate from the same liquid as that in which it was erupted, or fractionation of Ra from Ba during crystal growth was less effective than predicted from calculated partition coefficients.

Attributing the high $(^{226}\text{Ra})/\text{Ba}$ of the 1982 plagioclase to crystallization from another melt would require a much higher $(^{226}\text{Ra})/\text{Ba}$ in that melt than measured in any of the recent Mount St. Helens samples (see Table A1), and a very large excess of ^{226}Ra over ^{230}Th (of ~ 400 – 600%). Even allowing for a generous uncertainty in calculated $D_{\text{Ra}}/D_{\text{Ba}}$ ($\sim 25\%$, based on propagation of the 2σ extremes for all uncertainties in the calibrations of the elastic-strain model), the minimum $(^{226}\text{Ra})/(^{230}\text{Th})$ calculated for a liquid in equilibrium with plagioclase of this composition would be 3.3. Radium excesses of this magnitude are among the highest that have been measured in volcanic rocks (e.g. [21,22]) and therefore would require a magma that is not only unusual with respect to Mount St. Helens but also unusual with respect to volcanic rocks globally.

The alternative is that Ra and Ba were less efficiently fractionated during crystallization than theorized for chemical equilibrium. A potential mechanism to suppress equilibrium fractionation is suggested by the observation that extensive crystallization of plagioclase is inferred to have taken place over the course of the 1980–1986 eruptions of Mount St. Helens [23–25]. Trace-element concentrations at the crystal–liquid interface of growing crystals may be higher than

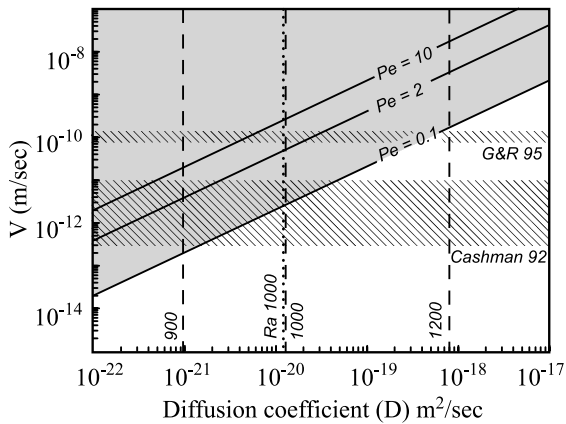


Fig. 6. Plot of diffusivity vs. growth rate illustrating conditions of potential growth entrapment. Solid lines represent contours of constant growth Peclet number $Pe = V/l/D_i$, where V is the crystal growth rate, l is the half-thickness of the enriched surface layer (assumed to be 50 Å), and D_i is the lattice diffusivity of element i [26]. Growth entrapment of element i will be measurable at $Pe = 0.1$, significant for $Pe > 2$, and $\sim 100\%$ effective (i.e. concentrations on the interior will be equal to those in the surface layer) at $Pe = 10$ [27]. Therefore, these values delimit regions of inefficient, partial, and efficient growth entrapment, respectively; the region where growth entrapment is possible is shaded. Estimates of plagioclase growth rates for the 1980–1986 dacite dome from Cashman [24] and Geschwind and Rutherford [25] are shown by labeled ruled fields. Experimentally determined diffusion coefficients for Ba in labradorite (An_{67}) from Cherniak [18] are shown by vertical dashed lines (labeled with temperatures in °C). Also shown is diffusion coefficient for Ra at 1000°C (dotted line) calculated by Cherniak using the method of Van Orman and others [19]. Based on these diffusivities and growth rates, growth entrapment is expected for crystallization at temperatures less than 1000°C, and could occur to some degree at temperatures up to 1200°C if growth rates were similar to maximum estimates.

bulk crystal–liquid equilibrium and these enrichments can be trapped if crystal growth rates are rapid relative to the diffusion rates of trace elements [26,27]. For the Mount St. Helens 1980–1986 dacite dome, plagioclase growth rates have been estimated to be 3×10^{-13} to 1.4×10^{-10} [24,25]. Using these estimates of growth rate, measured rates of Ba diffusion in plagioclase at magmatic temperatures [18], and estimated pre-eruptive temperatures of $\sim 900^\circ\text{C}$ [28], growth entrapment of Ba and Ra could have been significant during crystallization ($Pe > 0.1$; Fig. 6).

The general effect of growth entrapment should be to increase the relative abundances of incompatible elements like Ra, Ba, and Th in plagioclase, but the specific effect it would have on $(^{226}\text{Ra})/\text{Ba}$ and $(^{230}\text{Th})/\text{Ba}$ in plagioclase will depend on the difference between partitioning of those elements in the surface layer versus in the bulk crystal. Note that growth entrapment in this sense is an effect of the difference in equilibrium chemical behavior of trace elements in surface lattice sites compared to interior lattice sites and not to disequilibrium partitioning or physical entrapment of inclusions. Mineral–melt partitioning at the surface layer has not been quantified because the spatial resolution required to measure concentrations in the outermost layers of crystals is not available from any techniques currently in use [27]. However, it would seem likely that, as in the bulk equilibrium case, the extent of incorporation of an element into the surface layer of the crystal will depend on its charge and ionic radius. We speculate that the relatively open lattice sites in the surface layer compared to the interior will decrease distinctions in partitioning behavior of isovalent cations due to differences in ionic radius, but will have less of an effect on relative partitioning of elements with different valences. Thus, growth entrapment would likely lead to higher $(^{226}\text{Ra})/\text{Ba}$ but not necessarily $(^{230}\text{Th})/\text{Ba}$ in plagioclase at the time of crystal growth than that predicted from calculated bulk lattice partition coefficients.

One measure of the sensitivity of the Ra/Ba ratio to changes in the crystal lattice comes from the temperature dependence of that ratio. For example, the difference between the absolute magnitude of D_{Ba} and D_{Ra} at different temperatures is relatively small (less than a factor of 2 difference between 900 and 1100°C), but the corresponding differences in $D_{\text{Ra}}/D_{\text{Ba}}$ account for over half of the uncertainty in the age calculations. Thus, even if partitioning of Ra and Ba in the surface layer is not significantly different in absolute magnitude from that in the crystal interiors, growth entrapment could significantly affect $(^{226}\text{Ra})/\text{Ba}$ if it decreased the ability of the plagioclase lattice to discriminate between the two elements.

If growth entrapment has affected $(^{226}\text{Ra})/\text{Ba}$ in the 1982 plagioclase, then $(^{226}\text{Ra})/\text{Ba}$ predicted for a melt in equilibrium with plagioclase (Fig. 3A) would overestimate that of the actual melt from which the plagioclase crystals grew. The model crystallization age would therefore depend on the extent to which fractionation of Ra and Ba was less effective than predicted at equilibrium, itself a function both of the relative proportion of rapid crystallization to slower episodes of crystal growth and of the effectiveness of growth entrapment. For example, in the extreme case where there was no relative fractionation of Ra from Ba, the evolution curve for the melt in equilibrium with the plagioclase would coincide with the plagioclase evolution curve. Hence, the ('true') age of crystallization for plagioclase in the 1982 dacite would be that defined by the intersection between the plagioclase and whole rock evolution curves (1.7 ka; Table 3). If, instead, all crystallization occurred during ascent and eruption, the effective $D_{\text{Ra}}/D_{\text{Ba}}$ would have been ~ 0.4 rather than the predicted equilibrium value of ~ 0.2 . To put this another way, in the case of rapid, syn-eruptive overgrowth on older crystals, effective $D_{\text{Ra}}/D_{\text{Ba}}$ during the overgrowth would have to be > 0.4 in order to offset the lower $(^{226}\text{Ra})/\text{Ba}$ in the older cores expected due to aging. Thus, the average age of crystallization can be constrained to 0–1.7 ka and the effective $D_{\text{Ra}}/D_{\text{Ba}}$ during at least some period of crystallization to between 0.4 and 1. Because the TIMS data are from a mineral separate that largely includes phenocryst-sized ($> 100 \mu\text{m}$) material [9], one implication of this model would be that a substantial fraction of the volume of the plagioclase phenocrysts crystallized rapidly – either during ascent into a shallow crustal reservoir [29,30] or during final ascent and eruption – in addition to the rapid microlite and microphenocryst crystallization documented previously [23–25].

4.3.2. Rapid crystallization in older samples?

If the effect of rapid crystallization is to modify the initial Ra contents of crystals relative to Ba, it is worth also considering how the bulk crystal ages calculated for samples other than the 1982 dacite would be affected if growth entrapment

occurred in these samples during crystallization associated with ascent and eruption (cf. [23,31]). Had $(^{226}\text{Ra})/\text{Ba}$ in rapidly grown plagioclase been much higher than that predicted by partitioning, the curves for melt in equilibrium with plagioclase (Fig. 3) would 'overcorrect' for fractionation. This would have the effect of decreasing model ages relative to average crystallization ages, and thus the model ages can be considered minimum (average) ages of crystallization. There is, however, no specific evidence for rapid crystallization in these samples. Gardner and others [11] have suggested that higher crystallinity in mafic dacites ($< 64\%$ SiO_2) relative to more felsic dacites could reflect an origin by mixing of low- H_2O mafic magmas with felsic dacite melts, which would lower the overall water content and lead to plagioclase crystallization. If this is the case, then the relatively mafic 1982 dacite may have been more likely to have experienced rapid crystallization (immediately following mixing) than the more felsic Sugar Bowl dacite (MSH 90-7). In addition, given that the andesitic and basaltic magmas presented by the older samples likely were stored and erupted at higher temperature than the 1982 dacite, growth rates would have to have been comparable to or higher than the highest estimates of growth rate in Fig. 6 in order for growth entrapment to be effective. Therefore, the 1982 dacite might be expected to be more prone to rapid crystallization and associated growth entrapment than the other samples discussed here. Moreover, data for the plagioclase separates from all of the older lavas fall in a relatively restricted region of the ^{226}Ra – ^{230}Th isochron diagram (Fig. 1). This coherence may be more easily reconciled with a similar magnitude of ^{226}Ra –Ba fractionation than with a similar proportion of slow to rapid crystal growth.

4.4. Reconciling Ra–Th and Th–U ages

For three of the Mount St. Helens samples in this study, our ^{226}Ra – ^{230}Th model crystallization ages agree (within error) with the ^{230}Th – ^{238}U isochron ages based on data for the same minerals (Figs. 1 and 4; cf. V&H91). Exceptions, as was also noted by V&H91, are the 1982 dacite and the two oldest samples, the Castle Creek andesite and

basalt (MSH 90-2 and MSH 90-5, respectively). Whereas model plagioclase crystallization ages are $\sim 2\text{--}4$ ka for both Castle Creek samples, $^{230}\text{Th}/^{232}\text{Th}\text{--}^{238}\text{U}/^{232}\text{Th}$ data define linear arrays with apparent ages of 27 ± 12 and 34 ± 16 ka for the andesite and basalt, respectively (Fig. 1) [9]. Diffusion of Ra could lead to decoupling of $^{226}\text{Ra}\text{--}^{230}\text{Th}$ and $^{230}\text{Th}\text{--}^{238}\text{U}$ crystal ages and could apply to the Castle Creek basalt, where Ba concentrations measured in plagioclase from this sample are generally consistent with crystal–liquid equilibrium and pre-eruptive temperatures could have been high enough to allow relatively rapid diffusion. However, diffusion of Ra into or out of crystals in the Castle Creek andesite is unlikely to have been substantial considering the disequilibria in Ba between different zones within individual crystals.

The model preferred by V&H91 was that the apparent $^{230}\text{Th}\text{--}^{238}\text{U}$ isochrons represent mixing of older minerals (of unspecified age) with younger melts with higher $^{230}\text{Th}/^{232}\text{Th}$. Although V&H91 did not elaborate on this model, the following observations are pertinent. Plagioclase and olivine in the Castle Creek basalt (MSH 90-5) have identical $^{230}\text{Th}/^{232}\text{Th}$ within error (as expected of few-kyr-old minerals) and the slope of the apparent Th isochron is largely defined by the groundmass relative to the minerals. Plagioclase and pyroxene separates in the Castle Creek andesite (MSH 90-2) have measurably different $^{230}\text{Th}/^{232}\text{Th}$ but V&H91 describe the pyroxene separate as containing significant amounts of glass inclusions. Moreover, $(^{226}\text{Ra})/\text{Ba}$, $(^{230}\text{Th})/\text{Ba}$, $(^{230}\text{Th})/(^{232}\text{Th})$ and $(^{230}\text{Th})/(^{238}\text{U})$ in the pyroxene separate are all within error of the groundmass measurements even though Th/Ba in pyroxene measured by ion microprobe (Table 2) is much higher than that in the bulk separate, suggesting that budgets of Ra, Th, and U in the pyroxene separate are dominated by melt (either as inclusions or groundmass adhering to the outside of pyroxene grains). Thus, in both cases, mixing of 2–4 ka minerals with melts with higher $^{230}\text{Th}/^{232}\text{Th}$ is a viable model to explain the decoupling of $^{226}\text{Ra}\text{--}^{230}\text{Th}$ and (apparent) $^{230}\text{Th}\text{--}^{238}\text{U}$ ages.

Decoupling of $^{226}\text{Ra}\text{--}^{230}\text{Th}$ and $^{230}\text{Th}\text{--}^{238}\text{U}$ ages could also arise if the mineral separates are

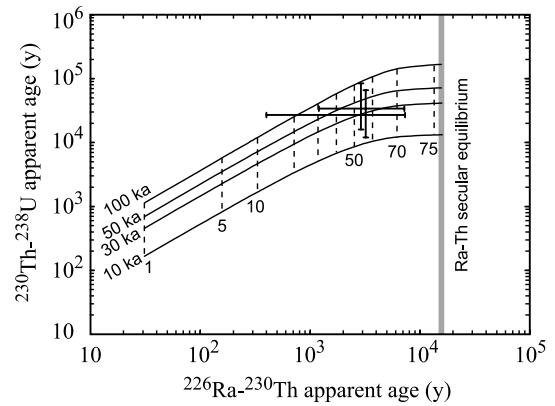


Fig. 7. Comparison of apparent $^{226}\text{Ra}\text{--}^{230}\text{Th}$ and $^{230}\text{Th}\text{--}^{238}\text{U}$ ages of plagioclase separates containing mixtures of old and young crystals. Curves are labeled to left with age of older episode of crystallization in ka (young crystals are assumed to be zero age) and dashed vertical lines indicate mass percentage of old crystallization in the mixture. Vertical gray bar indicates the oldest $^{226}\text{Ra}\text{--}^{230}\text{Th}$ age that can be distinguished analytically from secular equilibrium assuming initial $(^{226}\text{Ra})/(^{230}\text{Th})$ in plagioclase of 15 and analytical uncertainties of 1–2%. Also shown are $^{226}\text{Ra}\text{--}^{230}\text{Th}$ model ages and $^{230}\text{Th}\text{--}^{238}\text{U}$ apparent ages for the Castle Creek samples (crosses; length of lines indicates uncertainty). Old liquid and plagioclase are assumed to have started with the same $(^{230}\text{Th})/(^{238}\text{U})$ as that presently in the young liquid and plagioclase (i.e. that both old and young magma batches entered the reservoir system with the same initial $(^{230}\text{Th})/(^{238}\text{U})$), and present-day Ra concentrations in old plagioclase and liquid are calculated assuming equilibrium with ^{230}Th . Average ^{226}Ra and ^{230}Th concentrations in mixtures of old and young plagioclase are calculated by mass balance, and concentrations of Th, U, and Ba are assumed to be equal in old and young crystals. Apparent ages of plagioclase mixtures are calculated with reference to the young liquid using Eq. A4 in the Appendix, and using calculated partition coefficients for Ba and Ra for An₆₀ at 1000°C. Decoupling of $^{226}\text{Ra}\text{--}^{230}\text{Th}$ and $^{230}\text{Th}\text{--}^{238}\text{U}$ ages for Castle Creek samples could, for example, be explained by mixtures of approximately equal proportions of 30–50 ka crystals and zero age crystals.

mixtures of older and younger crystal populations (cf. [32]). Because different time scales are required for secular equilibrium to be attained between the two parent–daughter pairs, $^{226}\text{Ra}\text{--}^{230}\text{Th}$ ages of mixtures of crystals could be dominated by the young growth, whereas $^{230}\text{Th}\text{--}^{238}\text{U}$ ages could more closely reflect the bulk average age of crystallization and large discrepancies between the two apparent ages could be produced (Fig. 7).

One example of this type of scenario would be young overgrowths on older plagioclase crystals (whether early-formed phenocrysts or xenocrysts), which might be expected during degassing related to magma ascent. Because the difference between ^{226}Ra – ^{230}Th and ^{230}Th – ^{238}U ages in this model depends on a number of variables (the age of the old crystals, the proportion of old vs. young crystallization, and the relative concentrations of Th, U, and Ra in the old and young crystals (Fig. 7)), no unique solution to the specific proportions and ages of old and young growth can be determined from the apparent ages. However, considering that episodic or progressive growth will lead to Ra–Th model ages that are younger than the onset of crystallization (Fig. 5), the Ra–Th apparent ages are necessarily minimum ages for at least some zones or populations of the minerals. Even though they are non-unique, the illustrative calculations shown in Fig. 7 demonstrate that it is possible with this type of model to explain the combination of Ra–Th and Th–U ages that we observe as well as the decoupling of ages observed elsewhere (e.g. [1,33,34]).

4.5. Implications for magma reservoir processes

The relative ages of crystals erupted in different lavas from the same magmatic system, coupled with other geochemical information, can provide information about the dynamics of magma storage within the system. Model plagioclase ^{226}Ra – ^{230}Th crystallization ages for all samples (with the possible exception of the 1982 dacite) are broadly similar, with average ages of at least ~ 2 – 4 ka despite eruption ages that vary from 0.5 to 2 ka. The implication is that some significant mass fraction of plagioclase in all of these lavas crystallized at or before ~ 2 ka, which in turn implies that some crystals (or zones of crystals) in each magma were present beneath the volcano at ~ 2 ka. This observation could be consistent with two end-member scenarios: simultaneous storage and sequential eruption of separate magma batches, or entrainment of a significant population of crystals of similar age by successive magma batches.

If the Ra–Ba ages of the Mount St. Helens crystals reflect simultaneous storage of chemically

and isotopically [35] distinct magmas beneath the volcano, including those with different $^{230}\text{Th}/^{232}\text{Th}$ (Fig. 1), the distribution of magma within the reservoir system must be such that chemical heterogeneities are preserved while also maintaining magmatic temperatures for up to thousands of years. This may imply that the reservoir system resembles a plexus of closely spaced yet physically distinct pockets of magma rather than a large, open, well-mixed magma chamber. For the lavas more recent than Castle Creek time, which in this model would have been stored for up to 2 kyr longer than the older eruptions, $(^{226}\text{Ra})/(^{230}\text{Th})$ in parental magmas would have been a factor of ~ 2 – 3 higher than those measured, or 1.7–2.3. For reference, $(^{226}\text{Ra})/(^{230}\text{Th})$ in the Castle Creek olivine basalt corrected to the time of eruption was ~ 1.9 and significantly greater excesses have been obtained for other arc lavas [6,21,36]. Thus, ^{226}Ra excesses of the magnitude required for up to 2 kyr of storage could plausibly have been present in parental magmas.

If the crystal ages of the Mount St. Helens lavas instead reflect entrainment of a population of older crystals (cf. [11]), the different $^{230}\text{Th}/^{232}\text{Th}$ ratios of the plagioclase separates require that each magma entrained a similarly aged but distinct population of crystals. An intriguing, but somewhat speculative, possibility is that a significant percentage of plagioclase erupted in the various lavas represents recycling of material originally brought into the plumbing system during the Castle Creek period. This eruptive period appears to represent a dramatic shift in eruptive behavior for the volcano (e.g. [14,16,37]). Although it did not follow a particularly long dormant interval (only ~ 300 yr), the Castle Creek period marked a change from dominantly explosive and dacitic to silica-rich andesitic volcanism to a period dominated by effusive eruptions of mafic andesite and basalt, with minor dacite. Thus this period appears to have coincided with a major reorganization in the plumbing system of the volcano, and perhaps magmas with a wide diversity of Th isotopic compositions (similar to the diversity in the measured lavas) were either introduced into the system and/or were produced by varying degrees of interaction with the reser-

voir wallrocks. Crystals with these distinct compositions could have been preserved in the reservoir in a partially to completely crystallized magma and could have been remobilized and sampled by later magmas.

5. Conclusions

1. Variations in Ba concentration measured in plagioclase from recent Mount St. Helens samples are larger than expected from simple equilibrium partitioning and support previous interpretations of complex plagioclase crystal histories. This variability is evidence that plagioclase crystals were not in contact with their host liquids for long periods of time at high temperature (< 7 kyr at temperatures $> 1000^{\circ}\text{C}$) and that ^{226}Ra – ^{230}Th crystal ages have not appreciably been affected by diffusion of Ra into or out of the crystals. The Castle Creek basalt may be an exception to this.
2. When ^{226}Ra – ^{230}Th model crystallization ages are revised to reflect the effects of impurities in the mineral separates and the probable differential partitioning of Ra and Ba, no late-stage addition of Ra to the liquid after precipitation of the minerals is required.
3. Model plagioclase ages in all samples are similar and are older than ~ 2 ka, with the exception of the 1982 dacite. Consequently, a significant mass fraction of the *crystals* in each flow may have been stored concurrently beneath the volcano. This observation could imply simultaneous storage of physically distinct magma batches or incorporation of a population of similarly aged crystals into each successive magma batch.
4. High $(^{226}\text{Ra})/\text{Ba}$ in plagioclase in the 1982 dacite relative to the host liquid may reflect growth entrapment of surface enrichments during rapid crystallization, which we propose could lead to less discrimination between Ra and Ba than predicted by calculated bulk partition coefficients. If crystals in older lavas have also been influenced by growth entrapment, our model crystallization ages are minima.
5. We show that decoupling of ^{226}Ra – ^{230}Th and

^{230}Th – ^{238}U crystal ages can generally be explained by combinations of older and younger crystal growth from the same magma, but for the Castle Creek andesite and basalt could also be explained by mixing of crystals into melts with different $^{230}\text{Th}/^{232}\text{Th}$ ratios, as previously proposed.

6. References mentioned in the Appendix

[20,38]

Acknowledgements

We thank Alan Volpe for generously sharing his samples so that our analyses would be directly comparable to his previous work. We thank C. Coath and K. McKeegan for help with ion microprobe analyses, and M. Clynne and G. Gaetani for helpful discussions. We also thank Jon Blundy, Simon Turner, and Mark Reagan for constructive reviews that helped to refine and clarify the manuscript. This work was supported by NSF Grant EAR-9980646 (to M.R.R.) and a UCLA Dissertation-year fellowship to K.M.C. K.M.C. thanks the Division of Geological and Planetary Sciences at Caltech for a postdoctoral fellowship during the final stages of revision of the manuscript. The UCLA ion microprobe is partially subsidized by a grant from the National Science Foundation Instrumentation and Facilities Program. [BW]

References

- [1] S. Black, R. Macdonald, B. DeVivo, C.R.J. Kilburn, G. Rolandi, U-series disequilibria in young (A.D. 1944) Vesuvius rocks: Preliminary implications for magma residence times and volatile addition, *J. Volcanol. Geotherm. Res.* 82 (1998) 97–111.
- [2] K.W.W. Sims, D.J. DePaolo, M.T. Murrell, W.S. Baldrige, S. Goldstein, D. Clague, M. Jull, Porosity of the melting zone and variations in solid mantle upwelling rate beneath Hawaii: Inferences from ^{238}U – ^{230}Th – ^{226}Ra and ^{235}U – ^{231}Pa disequilibria, *Geochim. Cosmochim. Acta* 63 (1999) 4119–4138.
- [3] B. Bourdon, G. Worner, A. Zindler, U-series evidence for

- crustal involvement and magma residence times in the petrogenesis of Paríacota volcano, Chile, *Contrib. Mineral. Petrol.* 139 (2000) 458–469.
- [4] C.J. Hawkesworth, S. Blake, P. Evans, R. Hughes, R. Macdonald, L.E. Thomas, S.P. Turner, G. Zellmer, Time scales of crystal fractionation in magma chambers - integrating physical, isotopic and geochemical perspectives, *J. Petrol.* 41 (2000) 991–1006.
- [5] D. McKenzie, Constraints on melt generation and transport from U-series activity ratios, *Chem. Geol.* 162 (2000) 81–94.
- [6] S.P. Turner, R.M.M. George, P.J. Evans, C.J. Hawkesworth, G.F. Zellmer, Time-scales of magma formation, ascent and storage beneath subduction-zone volcanoes, *Philos. Trans. R. Soc. London A* 358 (2000) 1443–1464.
- [7] S.J. Schaefer, N.C. Sturchio, M.T. Murrell, S.N. Williams, Internal ^{238}U -series systematics of pumice from the November 13, 1985, eruption of Nevado del Ruiz, Colombia, *Geochim. Cosmochim. Acta* 577 (1993) 1215–1219.
- [8] M.K. Reagan, A.M. Volpe, K.V. Cashman, ^{238}U - and ^{232}Th -series chronology of phonolite fractionation at Mount Erebus, Antarctica, *Geochim. Cosmochim. Acta* 56 (1992) 1401–1407.
- [9] A.M. Volpe, P.E. Hammond, ^{238}U - ^{230}Th - ^{226}Ra disequilibria in young Mount St. Helens rocks: time constraint for magma formation and crystallization, *Earth Planet. Sci. Lett.* 107 (1991) 475–486.
- [10] K.M. Cooper, M.R. Reid, M.T. Murrell, D.A. Clague, Crystal and magma residence at Kilauea volcano, Hawaii: ^{230}Th - ^{226}Ra dating of the 1955 east rift eruption, *Earth Planet. Sci. Lett.* 184 (2001) 703–718.
- [11] J.E. Gardner, S. Carey, M.J. Rutherford, H. Sigurdsson, Petrologic diversity in Mount St. Helens dacites during the last 4,000 years: implications for magma mixing, *Contrib. Mineral. Petrol.* 119 (1995) 224–238.
- [12] J. Blundy, B. Wood, Prediction of crystal-melt partition coefficients from elastic moduli, *Nature* 372 (1994) 452–454.
- [13] B.J. Wood, J.D. Blundy, A predictive model for rare earth element partitioning between clinopyroxene and anhydrous silicate melt, *Contrib. Mineral. Petrol.* 129 (1997) 166–181.
- [14] D.R. Mullineaux, D.R. Crandell, The eruptive history of Mount St. Helens, in: P.W. Lipman, D.R. Mullineaux (Eds.), *The 1980 Eruptions of Mount St. Helens*, Washington, USGS Professional Paper 1250, US Government Printing Office, Washington, DC, 1981, pp. 3–15.
- [15] J.S. Pallister, R.P. Hoblitt, D.R. Crandell, D.R. Mullineaux, Mount St. Helens a decade after the 1980 eruptions: magmatic models, chemical cycles, and a revised hazards assessment, *Bull. Volcanol.* 54 (1992) 126–146.
- [16] J.T. Hagstrum, R.P. Hoblitt, C.A. Gardner, T.E. Gray, Holocene geomagnetic secular variation recorded by volcanic deposits at Mount St. Helens, Washington, *Bull. Volcanol.* 63 (2002) 545–566.
- [17] P.W. Layer, J.E. Gardner, Excess argon in Mount St. Helens plagioclase as a recorder of magmatic processes, *Geophys. Res. Lett.* 28 (2001) 4279–4282.
- [18] D.J. Cherniak, Ba diffusion in feldspar, *Geochim. Cosmochim. Acta* 66 (2002) 1641–1650.
- [19] J.A. Van Orman, T.L. Grove, N. Shimizu, Rare earth element diffusion in diopside: Influence of temperature, pressure and ionic radius, and an elastic model for diffusion in silicates, *Contrib. Mineral. Petrol.* 141 (2001) 687–703.
- [20] K.M. Cooper, Time scales of magma generation, differentiation, and storage: Constraints from Uranium-238-Thorium-230-Radium-226 disequilibria, Ph.D. Thesis, University of California, Los Angeles, 2001.
- [21] J.B. Gill, J.D. Morris, R.W. Johnson, Timescale for producing the geochemical signature of island arc magmas: U-Th-Po and Be-B systematics in recent Papua New Guinea lavas, *Geochim. Cosmochim. Acta* 57 (1993) 4269–4283.
- [22] S. Turner, P. Evans, C. Hawkesworth, Ultrafast source-to-surface movement of melt at island arcs from ^{226}Ra - ^{230}Th systematics, *Science* 292 (2001) 1363–1366.
- [23] K. Cashman, J. Blundy, Degassing and crystallization of ascending andesite and dacite, *Philos. Trans. R. Soc. London A* 358 (2000) 1487–1513.
- [24] K.V. Cashman, Groundmass crystallization of Mount St. Helens dacite, 1980-1986: a tool for interpreting shallow magmatic processes, *Contrib. Mineral. Petrol.* 109 (1992) 431–449.
- [25] C.H. Geschwind, M.J. Rutherford, Crystallization of microlites during magma ascent - the fluid-mechanics of 1980-1986 eruptions at Mount-St-Helens, *Bull. Volcanol.* 57 (1995) 356–370.
- [26] E.B. Watson, Y. Liang, A simple model for sector zoning in slowly grown crystals; implications for growth rate and lattice diffusion, with emphasis on accessory minerals in crustal rocks, *Am. Mineral.* 80 (1995) 1179–1187.
- [27] E.B. Watson, Surface enrichment and trace-element uptake during crystal growth, *Geochim. Cosmochim. Acta* 60 (1996) 5013–5020.
- [28] M.J. Rutherford, P.M. Hill, Magma ascent rates from amphibole breakdown: an experimental study applied to the 1980-1986 Mount St. Helens eruption, *J. Geophys. Res.* 98 (1993) 19667–19686.
- [29] J.D. Blundy, R.S.J. Sparks, C. Annen, R.A. Brooker, O. Melnik, K.V. Cashman, Generation, ascent and crystallization of calc-alkaline silicic magmas, *Geochim. Cosmochim. Acta* 66 (2002) A83.
- [30] J. Blundy, K. Cashman, Ascent-driven crystallisation of dacite magma at Mount St Helens, 1980-1986, *Contrib. Mineral. Petrol.* 140 (2001) 631–650.
- [31] T. Kuritani, Phenocryst crystallization during ascent of alkali basalt magma at Rishiri Volcano, northern Japan, *J. Volcanol. Geotherm. Res.* 88 (1999) 77–97.
- [32] B. Charlier, G. Zellmer, Some remarks on U-Th mineral ages from igneous rocks with prolonged crystallization histories, *Earth Planet. Sci. Lett.* 183 (2000) 457–469.
- [33] A.M. Volpe, ^{238}U - ^{230}Th - ^{226}Ra disequilibrium in young

- Mt. Shasta andesites and dacites, *J. Volcanol. Geotherm. Res.* 53 (1992) 227–238.
- [34] E. Heath, S.P. Turner, R. Macdonald, C.J. Hawkesworth, P. van Calsteren, Long magma residence times at an island arc volcano (Soufriere, St. Vincent) in the Lesser Antilles: evidence from ^{238}U - ^{230}Th isochron dating, *Earth Planet. Sci. Lett.* 160 (1998) 49–63.
- [35] A.N. Halliday, A.E. Fallick, A.P. Dickin, A.B. Mackenzie, W.E. Stephens, W. Hildreth, The isotopic and chemical evolution of Mount St. Helens, *Earth Planet. Sci. Lett.* 63 (1983) 241–256.
- [36] P.-J. Gauthier, M. Condomines, ^{210}Pb - ^{226}Ra radioactive disequilibria in recent lavas and radon degassing: inferences on the magma chamber dynamics at Stromboli and Merapi volcanoes, *Earth Planet. Sci. Lett.* 172 (1999) 111–126.
- [37] D.R. Crandell, Deposits of pre-1980 pyroclastic flows and lahars from Mount St. Helens Volcano, Washington, US Geological Survey Professional Paper 1444 (1987).
- [38] H. Cheng, R.L. Edwards, J. Hoff, C.D. Gallup, D.A. Richards, Y. Asmerom, The half-lives of uranium-234 and thorium-230, *Chem. Geol.* 169 (2000) 17–33.